


Origin of the enhanced ferroelectricity in multiferroic SmMn_2O_5

S. Mansouri ^{1,2,*}, S. Jandl,¹ M. Balli,^{1,3} P. Fournier,¹ Y. Ishii,⁴ H. Kimura,⁵ M. Orlita,^{6,7} and M. Chaker²

¹Regroupement québécois sur les matériaux de pointe et Institut Quantique, Université de Sherbrooke, Département de Physique, Sherbrooke, Québec, Canada J1K 2R1

²Centre Énergie, Matériaux et Télécommunications, Institut National de la Recherche Scientifique, 1650, Boulevard Lionel-Boulet, Varennes, Québec, Canada J3X 1S2

³LERMA, ECINE, International University of Rabat, Parc Technopolis, Rocade Rabat-Salé 11100, Morocco

⁴Condensed Matter Research Center and Photon Factory, Institute of Materials Structure Science, High Energy Accelerator Research Organization (KEK), Tsukuba, Ibaraki 305-0801, Japan

⁵Institute of Multidisciplinary Research for Advanced Materials, Tohoku University, Sendai 980-8577, Japan

⁶Laboratoire National des Champs Magnétiques Intenses, CNRS-UGA-UPS-INS-EMFL, 25 rue des Martyrs, 38042 Grenoble, France

⁷Faculty of Mathematics and Physics, Charles University, Ke Karlovu 5, 121 16 Prague 2, Czech Republic



(Received 13 June 2019; published 30 August 2019)

In orthorhombic SmMn_2O_5 single crystals, Sm^{3+} crystal-field (CF) excitations are studied by infrared transmission as a function of temperature and under applied magnetic field up to 10 T. These measurements are complemented with the study of Raman-active phonon frequency shifts as a function of temperature between 300 and 5 K. The frequencies of all 6H_j crystal-field levels of Sm^{3+} were determined as well as those of 6F_j . At high temperatures, the evolutions of Sm^{3+} CF excitations exhibit anomalies around the characteristic temperatures, $T^* \sim 60$ K and $T^S \sim 120$ K and reflect the thermal disorder induced by splitting of the Sm-O bonds in SmMn_2O_5 that contribute to the frequency and linewidth phonon shifting. At low temperatures, the degeneracy of the ground-state Kramers doublet is lifted ($\Delta_0 \sim 36 \text{ cm}^{-1}$) due to the Sm^{3+} - Mn^{3+} interaction in the ferroelectric phase and strongly enhanced below $T_C \sim 26$ K. The Sm-Mn exchange interaction J_6 is determined and compared to that of Gd-Mn interaction in GdMn_2O_5 . The Sm magnetic moment $m_{\text{Sm}}(T)$ and the Sm contribution to the magnetic susceptibility are also evaluated from $\Delta_0(T)$, indicating that the Sm-Mn interaction is strongly implicated in the magnetic and the ferroelectric orderings below ~ 26 K. The study of the Sm^{3+} CF excitations as a function of magnetic field reveals twinning in SmMn_2O_5 . This twinning could affect its electric polarization behavior versus magnetic field.

DOI: [10.1103/PhysRevB.100.085147](https://doi.org/10.1103/PhysRevB.100.085147)

I. INTRODUCTION

Ferroelectric magnets, especially of type II, are a fascinating class of materials: The occurrence of the ferroic order requires a particular spin arrangement that breaks the inversion symmetry [1]. These materials have attracted great attention as they are candidates for the next generation of data storage devices [2–7]. Manganite RMnO_3 and RMn_2O_5 are prototype materials of multiferroics of type II [2–4]. The strong coupling between the ferroelectric order and the magnetic order is attributed to different mechanisms: the inverse Dzyaloshinskii-Moriya interaction model [8], spin-current model [9], the exchange-striction mechanism [3,4,10,11] and the spin-dependent metal-ligand hybridization model [12–15]. In RMnO_3 , the spontaneous electric polarization \mathbf{P} is given by $\mathbf{P} \propto \mathbf{S}_i \times \mathbf{S}_j$, where \mathbf{S}_i and \mathbf{S}_j are adjacent Mn spins that form a magnetic spiral order [8,9]. In comparison, the ferroelectricity in RMn_2O_5 is rather attributed to a symmetric exchange interaction where $\mathbf{P} \propto \mathbf{S}_i \cdot \mathbf{S}_j$ [10]. For both families, the proposed models suggest that the magnitude of \mathbf{P} depends mainly on the Mn-Mn magnetic interaction. However, many

studies demonstrated a significant contribution of rare-earth spins, direct and indirect, to electric polarization in RMnO_3 and RMn_2O_5 [11,16–21]. Indirectly, the contribution of R ions, through the R -Mn interaction, on the magnetoelectric coupling in RMnO_3 is found in the flop of the Mn cycloid moments into the ab plane that reorients the spontaneous electric polarization from the c axis to the a axis [2,16]. Furthermore, the enhancement of \mathbf{P} in DyMnO_3 is found to be quantitatively coupled to the ordering of Dy spins along the b axis [17]. This important contribution is explained by Dy spin ordering that enhances the amplitude of the Mn spin spiral [17]. Similar findings are also observed in the RMn_2O_5 multiferroics [3,11,18–21]. The influence of R spins ordering upon the magnetic ordering of Mn spins, hence the magnetoelectric coupling, can be clearly observed in the difference between the multiferroic properties of RMn_2O_5 with magnetic and nonmagnetic R ions [3,10]. For example, in TbMn_2O_5 , the spontaneous electric polarization is positively enhanced in the low-temperature phase [3,11], while it decreases and reaches a negative value for Ym_2O_5 [10]. Also, the particular increasing of TbMn_2O_5 electric polarization below 15 K up to $\sim 40 \text{ nC cm}^{-2}$ at 5 K coincides with the increase of the Tb^{3+} magnetic moment observed by neutron scattering [18], suggesting a strong coupling between \mathbf{P}_b and Tb^{3+} spins. Recent

*saber.mansouri@usherbrooke.ca

studies on DyMn_2O_5 have also revealed that its electric polarization is finely tuned depending on the symmetric exchange striction of the Dy-Mn interaction [19,20]. Similar effects are also observed in GdMn_2O_5 and SmMn_2O_5 [21–24]. There is thus some real interest in understanding the magnetic coupling between R and Mn spins $J_{\text{Mn}-R}$ and its actual contribution to the multiferroic properties of RMn_2O_5 .

SmMn_2O_5 represents a particular case of the RMn_2O_5 family members due to its unique orientation of the magnetic moments [22,24]. Indeed, Yahia *et al.* [22] and Ishii *et al.* [24] have newly determined that the magnetic moments are perfectly aligned in SmMn_2O_5 , and the Sm and Mn magnetic moments have a dominant c -axis component, which is quite unique because Mn moments have a dominant a -axis component in other RMn_2O_5 (R = rare earth, Y, Bi) compounds. This particular case rules out the possible Dzyaloshinskii-Moriya interaction scenario and suggests that the mechanism responsible for the spin-induced electric polarization in the RMn_2O_5 series is the exchange-striction model. In SmMn_2O_5 , heat-capacity measurements have shown three anomalies at $T_1 = 35 \pm 2$ K, $T_2 = 28 \pm 2$ K, and $T_3 = 6 \pm 2$ K [25]. Previous dielectric constant and electric polarization measurements, done on our SmMn_2O_5 samples, have revealed that two peaks diverge at T_1 and T_2 [24]. These peaks correspond to the occurrence of a weak electric polarization below T_1 , significantly enhanced below T_2 . In addition, T_1 matches well with a subtle anomaly observed in the magnetic susceptibility (χ) along the a axis [24] and T_2 coincides with a significant increase (small decrease) of χ along the a axis (along the c axis), while T_3 corresponds to a notable decrease of χ along the c axis.

Few techniques are sensitive tools to structural and magnetic properties as well as local anisotropic interactions and electronic and magnetic excitations, such as neutron diffraction. Infrared and Raman-scattering techniques have been successfully used for the study of the coupling between charge, spin, and lattice degrees of freedom in strongly correlated electron systems such as high-temperature superconductors and manganite materials [26–30]. Indeed, the evolution of the phonon and crystal-field (CF) excitation characteristics as a function of temperature and magnetic field reveals interesting information on the magnetic interactions and the electronic properties as well as the surrounding ligands and the local inhomogeneities [31]. In particular, the Nd^{3+} , Sm^{3+} , and Dy^{3+} Kramers ions, with odd numbers of electrons in their $4f$ shell, have levels with twofold degeneracies when they are located inside a crystal with low site symmetry. A lifting of the Kramers degeneracy is only possible by means of additional perturbation, which breaks the time-reversal invariance of the rare-earth-ion Hamiltonian, such as magnetic interactions with other atoms in the crystal or an external magnetic field. The high sensitivity of the Kramers-ion crystal-field levels to both the local electric and magnetic fields, combined with the high resolution of the spectroscopic techniques, makes it a valuable probe for existing magnetic exchanges in SmMn_2O_5 . Another reason to perform a spectroscopic study of SmMn_2O_5 CF transitions is the fact that Sm, in its natural isotopic abundance, is a very strong neutron absorber. This makes inelastic neutron-scattering (INS) spectroscopy only possible for Sm isotope-enriched samples, and up to now there is no INS

study reported for ^{154}Sm -enriched SmMn_2O_5 compounds. Additionally, usually only CF transitions within the lowest J multiplet are accessible in INS studies, while observations of intermultiplet transitions are scarce. In contrast, infrared transmission technique can offer more empirical data that could be helpful for future reliable CF parameter estimations.

To our knowledge, there is no information in the literature about the Sm^{3+} crystal-field scheme for SmMn_2O_5 . In this paper, we present mainly a detailed study of the Sm^{3+} CF excitations in SmMn_2O_5 single crystals, as a function of temperature and under applied magnetic field (at 4.2 K). These experiments are complemented with Raman measurements of SmMn_2O_5 . The main objective of this paper is to probe the role of the coupling between Sm $4f$ and Mn $3d$ moments in the multiferroic properties of SmMn_2O_5 . This objective is addressed by studying the Sm^{3+} Kramers-doublet (KD) excitation responses that are sensitive to intrinsic magnetic interactions and external magnetic field as well as to local disorders of the surrounding ligands in SmMn_2O_5 .

II. EXPERIMENT

SmMn_2O_5 single crystals were grown with the flux-melt method [24,32]. The flux was maintained at 1150°C for 20 h and gradually cooled to 950°C at a rate of $1.2^\circ\text{C}/\text{h}$. The x-ray single-crystal structural analysis indicates that SmMn_2O_5 crystallizes with the lattice parameters $a = 7.425 \text{ \AA}$, $b = 8.596 \text{ \AA}$, and $c = 5.672 \text{ \AA}$ at room temperature [24]. The Raman spectra were obtained using a Labram-800 Raman spectrometer equipped with a nitrogen-cooled charge-coupled device detector. SmMn_2O_5 samples were placed on the cold finger of a microhelium Janis cryostat and the Raman spectra were measured between 300 and 5 K. The exciting laser (632.8 nm) was forwarded through a $50\times$ objective with weak intensity, less than 0.8 mW, to avoid local heating. The infrared transmission spectra were recorded in the $1500\text{--}8000 \text{ cm}^{-1}$ range with a Fourier transform interferometer BOMEM DA3.002 equipped with a quartz-halogen source, a CaF_2 beamsplitter, and an InSb detector. For experiments in magnetic field, the sample was placed in a cryostat equipped with a superconducting coil (B parallel to the c axis of the sample), which was coupled via light-pipe optics to a Bruker Vertex 80v spectrometer. The sample was kept at 4.2 K in a low-pressure helium gas during the experiments.

III. RESULTS AND DISCUSSION

The RMn_2O_5 series crystallize in the orthorhombic structure [33] where edge-shared Mn^{4+}O_6 octahedra are linked along the c axis and pairs of Mn^{3+}O_5 pyramids are connected to two Mn^{4+}O_6 chains. The R ions are sited in distorted RO_8 polyhedra. Figure 1 shows the Raman spectra of SmMn_2O_5 which reproduce the typical Raman signature of other orthorhombic RMn_2O_5 manganites as previously reported in Refs. [27] and [31]. The Raman spectra of SmMn_2O_5 are sensitive to $x(\text{z}z)x$ and $x(\text{y}'z')x$ configurations and the linewidths of detected phonons are close to $3\text{--}9 \text{ cm}^{-1}$ attesting to the high crystalline quality of our samples. With decreasing temperature, between 300 and 5 K, no additional modes appear suggesting also a structural phase stability of the samples.

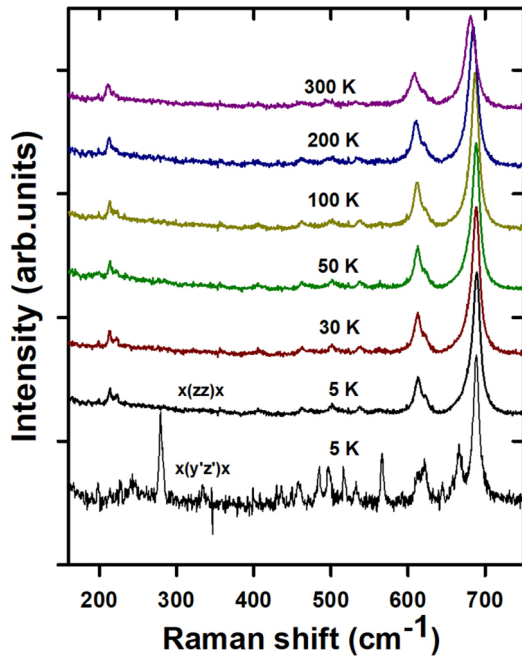


FIG. 1. Temperature dependence of the Raman spectra of SmMn_2O_5 in $x(y'z')x$ and $x(zz)x$ (at 5 K) configurations.

Figure 2 shows the thermal evolution of the Raman frequencies of the 213 cm^{-1} [2(a)], 615 cm^{-1} [2(b)], 624 cm^{-1} [2(c)], 667 cm^{-1} [2(d)], and 691 cm^{-1} [2(e)] modes in SmMn_2O_5 .

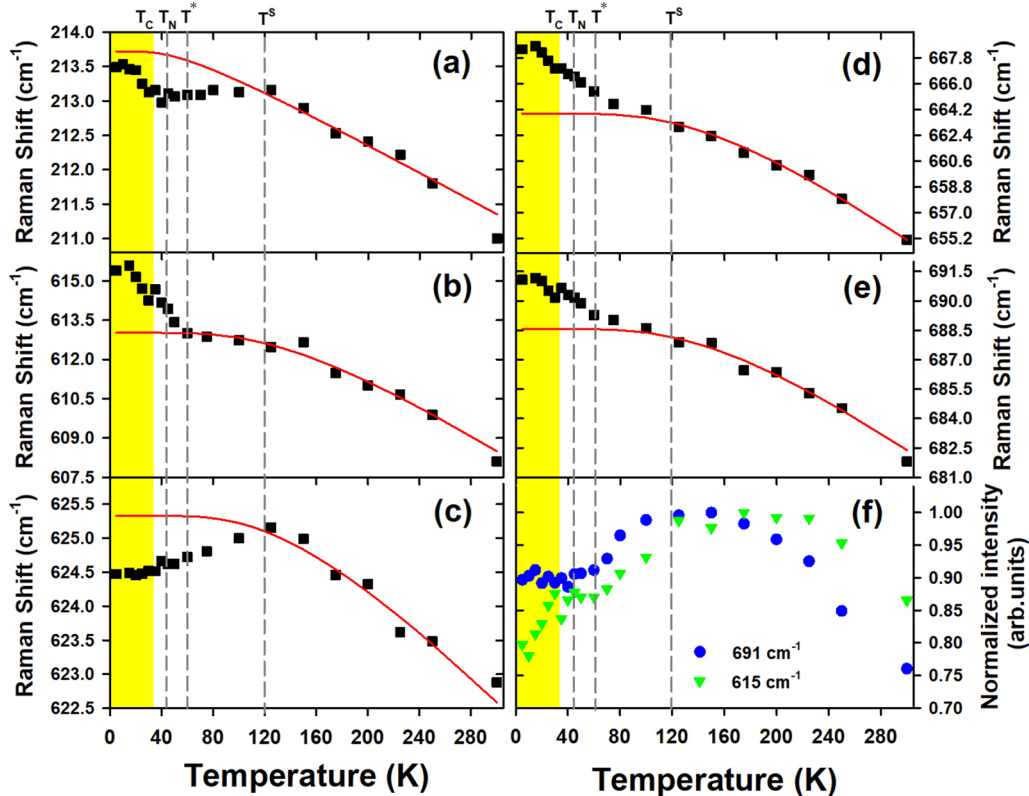


FIG. 2. Thermal evolution of the Raman frequency of the 213 cm^{-1} (a), 615 cm^{-1} (b), 624 cm^{-1} (c), 667 cm^{-1} (d), and 691 cm^{-1} (e) modes and the normalized integrated intensity (f) of the 691 cm^{-1} mode in SmMn_2O_5 . Dotted lines correspond to the anharmonic behavior. The dashed lines indicate the characteristic temperatures T_C , T_N , T^* , and T^S defined in the text.

The temperature dependence of the normalized integrated intensities of the 615 and 691 cm^{-1} modes is also presented in Fig. 2(f). Its variations exhibit subtle anomalies around the characteristic temperatures, $T_C \sim 34\text{ K}$, $T^* \sim 60\text{ K}$, and $T^S \sim 120\text{ K}$. Remarkably, the Raman frequency of the $\sim 691\text{ cm}^{-1}$ mode increases between 300 and 140 K and decreases significantly below $T^S \sim 120\text{ K}$. Similar thermal behavior has also been observed for the Raman modes at ~ 220 , ~ 327 , and $\sim 700\text{ cm}^{-1}$. These observations are similar to what we have recently reported for NdMn_2O_5 [34], TbMn_2O_5 , HoMn_2O_5 , and YMn_2O_5 compounds [31]. We have identified the characteristic temperature at $T^S \sim 140\text{ K}$ as the result of common local distortions in RMn_2O_5 induced by the splitting of R -O links, in short and long bonds. This local thermal disorder in the rare-earth sites is reduced at $T^* \sim 60\text{ K}$ when the number of the short bonds matches up the number of the long bonds in the unit cell [31].

The Sm^{3+} ion has 5 electrons in its $4f$ shell which are responsible for its magnetic properties. According to Hund's rules, the lowest spectroscopic term is 6H ($S = 5/2$ and $L = 5$, where S and L are, respectively, the spin and the orbital angular momentum quantum numbers). The spin-orbit interaction splits this term into multiplets which have J values ranging from $(L-S)$ to $(L+S)$, i.e., 6H_j term with $J = 7/2$, $J = 9/2$, $J = 11/2$, $J = 13/2$, and $J = 15/2$. Additionally, we note that for the higher $\text{Sm } {}^6H_j$ multiplets there is an admixture of levels with the 6F term. In orthorhombic SmMn_2O_5 , the Sm^{3+} ions are located on sites with C_s^{xy}

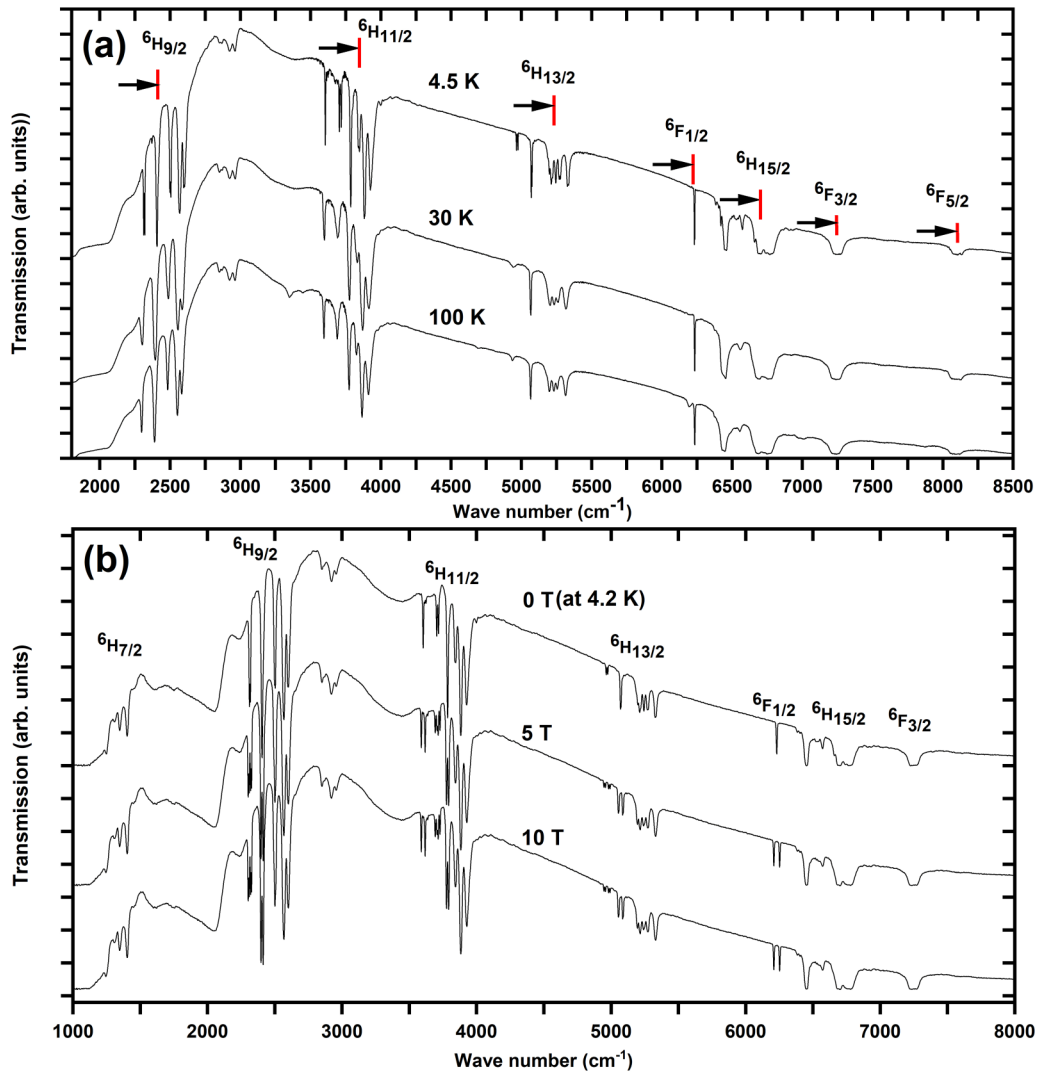


FIG. 3. Transmission spectra of SmMn₂O₅ as a function of temperature (a), at 4.5, 30, and 100 K, and under applied magnetic field (b) at 0, 5, and 10 T (at 4.2 K).

symmetry. Each multiplet is thus split to $(2J + 1)/2$ sublevels or Kramers doublets due to the crystal-field effect of surrounding oxygen atoms. Figures 3(a) and 3(b) present, respectively, selected transmission spectra of SmMn₂O₅ as a function of temperature, at 4.5, 30, and 100 K, and of magnetic field at 0, 5, and 10 T. Six groups of sharp absorption lines due to f - f transitions of Sm³⁺, centered at 1400, 2500, 3850, 5250, and 6650 cm⁻¹ are detected as theoretically predicted for the absorption bands of the ${}^6H_{5/2} \rightarrow {}^6H_{7/2}$, ${}^6H_{5/2} \rightarrow {}^6H_{9/2}$, ${}^6H_{5/2} \rightarrow {}^6H_{11/2}$, ${}^6H_{5/2} \rightarrow {}^6H_{13/2}$, and ${}^6H_{5/2} \rightarrow {}^6H_{15/2}$ CF transitions. Other absorption bands around 6230, 7250, and 8100 cm⁻¹ are also observed. These bands correspond to the lowest ${}^6F_{j=1/2, 3/2, \text{ and } 5/2}$ multiplets of the spectroscopic term 6F . Table I lists the CF energy levels of both the 33 Kramers doublets of Sm³⁺ 6H_j term and the 6 Kramers doublets of Sm³⁺ ${}^6F_{j=1/2, 3/2, \text{ and } 5/2}$ multiplets in SmMn₂O₅. As expected, our measurements confirm the admixture of the higher Sm 6H_j multiplets with the lowest levels of the 6F term. The ${}^6H_{5/2}$ ground-state excited levels are determined when they are thermally populated, at high temperatures above 100 K. Their energy values are deduced from the comparison between the

thermally excited levels of the 6H_j multiplets ($J = 9/2, 11/2,$ and $13/2$). The determination of the CF level frequencies is necessary for the success of the numerical search for reliable CF parameters that depends strongly on the initial estimate.

At high temperature, between 300 and 35 K, the evolutions of all Sm³⁺ CF excitations exhibit anomalies around the characteristic temperatures, $T^* \sim 60$ K and $T^S \sim 120$ K. An example of the temperature dependence of the frequency and the full width at half maximum (FWHM) of all CF excitations of the ${}^6H_{9/2}$ multiplet are reported in the Supplemental Material in Fig. S1 [35]. The frequency of all CF excitations is nearly constant between 300 and 120 K and hardens significantly below 60 K. Interestingly, the FWHM of all ${}^6H_{9/2}$ CF excitation decreases progressively between 300 and ~ 120 K and increases considerably between 60 and 35 K. A similar behavior has also been observed for the FWHM of the Nd³⁺ KD CF excitations in NdMn₂O₅ [34]. Broadenings of the Sm³⁺ CF excitations are also similar to what we have recently reported for the non-Kramers Tb³⁺ and Ho³⁺ CF excitations in TbMn₂O₅ and HoMn₂O₅ [31]. These overall findings are explained by a local disorder effect induced by the splitting

TABLE I. Experimental CF energy levels (cm^{-1}) at 100 K of the Kramers doublets of Sm^{3+} in SmMn_2O_5 .

CF levels	${}^6H_{5/2}$	${}^6H_{7/2}$	${}^6H_{9/2}$	${}^6H_{11/2}$	${}^6H_{13/2}$	${}^6F_{1/2}$	${}^6H_{15/2}$	${}^6F_{3/2}$	${}^6F_{5/2}$
Energy (cm^{-1})	0	1252 ^b	2298	3595	4937	6232	6433	7222	8052
	144 ^a	1310 ^b	2390	3690	5067		6448	7255	8076
	242 ^a	1348 ^b	2484	3775	5177		6560		8114
		1404 ^b	2552	3827	5200		6674		
			2583	3866	5231		6694		
				3912	5257		6722		
					5315		6750		
							6776		

^aThe energy of ${}^6H_{5/2}$ CF excitations is determined when they are thermally populated.

^bThe energy of ${}^6H_{7/2}$ CF transitions is determined at 4.2 K.

of R - O bonds into short and long bonds that also explains the decrease of the Raman intensities and the frequency shifts of some RMn_2O_5 phonons at relatively high temperatures. These observations confirm again the universal behavior of the RMn_2O_5 lattice dynamic properties and call into question the relationship between the thermal dynamic of the R - O bonds and the ferroelectric properties in the RMn_2O_5 systems at high temperatures [36–38]. We suggest that the thermal disorder effect induced by the R - O bond splitting involves a small deviation of the R^{3+} ions from its centrosymmetric site in $P6mm$ space group that renders difficult the determination of the actual space-group symmetry of RMn_2O_5 systems at high temperature as previously reported by Baledent *et al.* [36].

Figures 4(a) and 4(b) show the absorbance spectra of Sm^{3+} ${}^6H_{5/2} \rightarrow {}^6H_{9/2}$ and ${}^6H_{5/2} \rightarrow {}^6H_{11/2}$ CF transitions as a function of temperature, between 100 and 4.5 K. The absorbance spectra (A) are calculated from the transmission spectra (T) and the incident intensity (I_0) using the equation $A = -\log_{10}(T) = -\log_{10}(I/I_0)$. The dashed lines indicate the positions of the different CF transitions. Below 35 K, exactly at the occurrence of the ferroelectric phase transition, the different lines are equally split compared to their initial positions. For example, at 33 K the doublet frequencies for the ${}^6H_{9/2}$ multiplets are ~ 2298 – 2306 , ~ 2389 – 2397 , ~ 2483 – 2491 , 2549 – 2557 , and 2586 – 2594 cm^{-1} . In addition, all the observed lines behave the same way with decreasing temperature. The temperature dependence of the splitting shift is the same for all the CF excitations. Also, the spectral weight of each excitation component is shifted at higher frequency with decreasing temperature. All these observations indicate clearly that the main contribution to the line splitting arises from the lifted degeneracy of the KD ground state. Below 27 K, the magnitude of the ground-state splitting (Δ_0) is strongly enhanced and reaches ~ 36 cm^{-1} at 4.5 K. A representative absorbance map of Sm^{3+} ${}^6H_{5/2} \rightarrow {}^6H_{9/2}$ CF transitions as a function of temperature, between 40 and 4.5 K, is shown in Fig. S2(a) reported in the Supplemental Material [35]. An additional splitting of some CF excitations, with different Δ_i' magnitudes inferior to the one of the KD ground state Δ_0 , is also observed below 26 K, such as the CF excitation around 2298, 2484, and 2583 cm^{-1} . For example, the band at 2298 cm^{-1} is resolved in bands at ~ 2283 cm^{-1} and ~ 2313 cm^{-1} below 26 K. As the temperature is lowered, these two bands split, in their turn, into two other close bands at 2277–2284 cm^{-1} and ~ 2311 – 2318 cm^{-1} at 22 K. These

results confirm the splitting of the two Kramers doublets: the Sm^{3+} KD ground state and the excited KD level at 2298 cm^{-1} . These experimental results are in agreement with the expected prediction as illustrated in the inset of Fig. 4. The four arrows indicate all possible CF transitions. Such detailed scheme is not evident for all excited levels due to their relatively broad widths which are related to their own Landé g_z factor. The change of spectral weight, between the KD components, is due to the depletion of the ground-state excited-level KD with decreasing temperature. As expected, such change of spectral

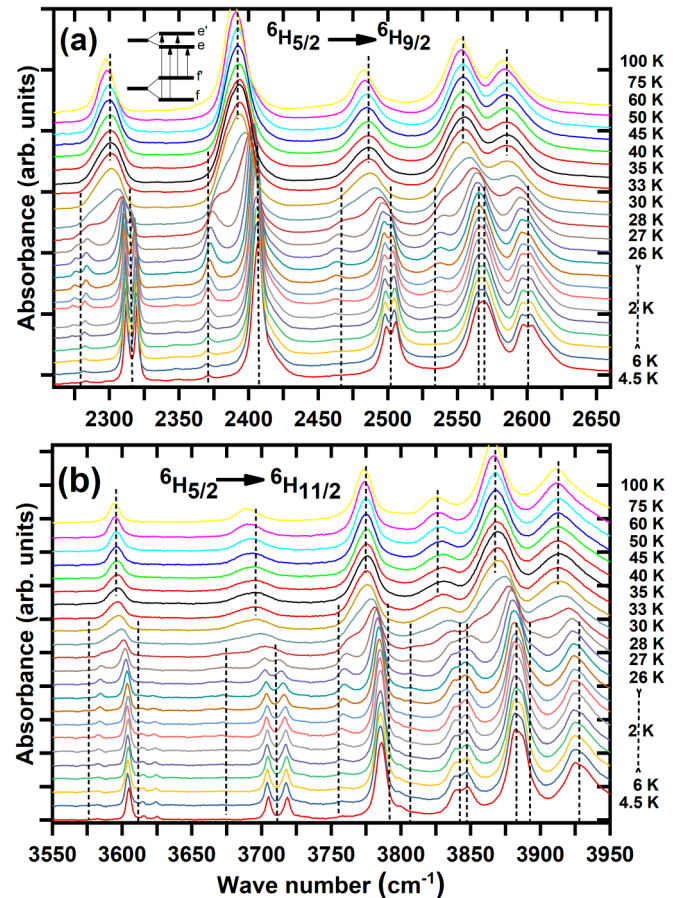


FIG. 4. Absorbance spectra of Sm^{3+} ${}^6H_{5/2} \rightarrow {}^6H_{9/2}$ and ${}^6H_{5/2} \rightarrow {}^6H_{11/2}$ CF transitions as a function of temperature, between 100 and 4.5 K in SmMn_2O_5 .

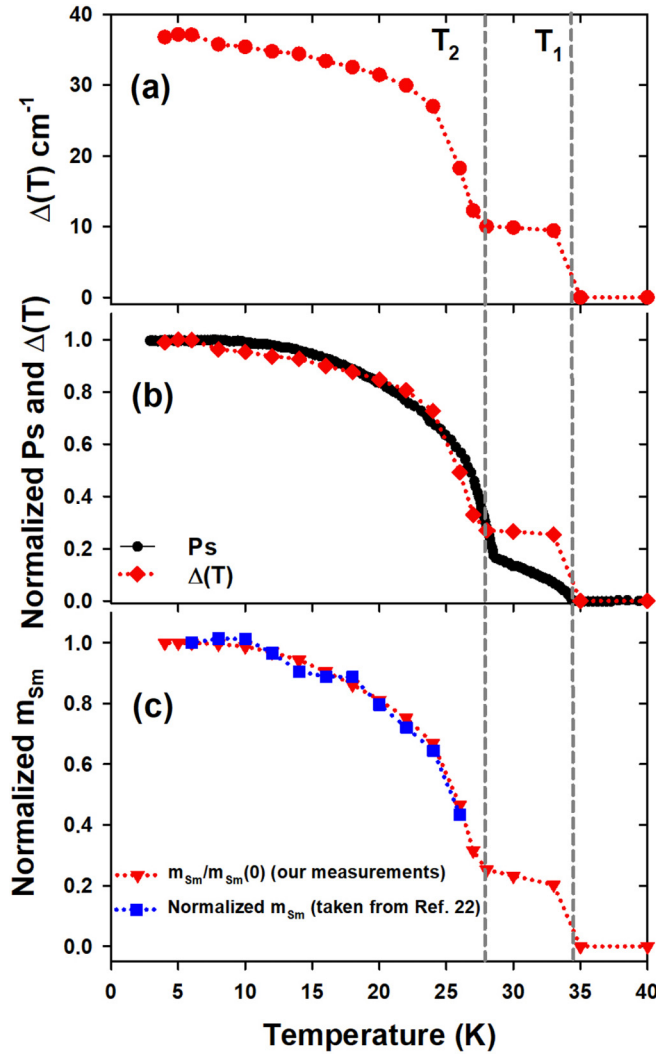


FIG. 5. (a) Variation of the splitting $\Delta_0(T)$ as a function of temperature. (b) Normalized data of the electric polarization P_s and the splitting $\Delta_0(T)$ with respect to their values at 4.5 K. (c) Temperature dependence of $m_{\text{Sm}}(T)/m_{\text{Sm}}(0)$ calculated from $\Delta_0(T)$ using Eq. (2) and compared to its direct measurements by neutron diffraction.

weight is not observed between the components of the excited KD depending on the transition probabilities.

The variation of $\Delta_0(T)$ as a function of temperature is presented in Fig. 5(a). The Sm^{3+} ground Kramers doublet splits below $T_C \sim 34$ K, precisely in the ferroelectric phase. The magnitude of this splitting is strongly enhanced below $T_2 \sim 27$ K and reaches $\Delta_0 \sim 36 \text{ cm}^{-1}$ at 4.5 K. Remarkably, this magnitude of the ground-state splitting is more important than that observed in NdMn_2O_5 ($\Delta_0 \sim 7.5 \text{ cm}^{-1}$) [34]. This is related to the unique orientation of the magnetic moments in SmMn_2O_5 , where Sm and Mn magnetic moments exhibit perfectly collinear moments oriented along the c axis, which creates an important effective magnetic field at different Sm sites compared to the usual ab -plane anisotropy of the magnetic moments in the other RMn_2O_5 members of the series. In the following, we calculate the samarium magnetic moment $m_{\text{Sm}}(T)$ and the samarium contribution

to the magnetic susceptibility using $\Delta_0(T)$ dependence. At mean-field level, the splitting $\Delta_0(T)$ and the Sm^{3+} magnetic moment can be written according to the following equations [20]:

$$\Delta \approx zJ_6 \langle m_{\text{Mn}} \rangle 2 \frac{m_{\text{Sm}}(0)}{g_J}, \quad (1)$$

$$m_{\text{Sm}}(T)/m_{\text{Sm}}(0) = \tanh[-\Delta_0(T)/2k_B T], \quad (2)$$

where J_6 is the Sm-Mn exchange interaction, $g_J = 2/7$ is the Landé factor, $z = 2$ is the number of Mn^{3+} neighbors of a given Sm^{3+} spin, $\langle m_{\text{Mn}} \rangle$ is the average Mn^{3+} magnetic moment, k_B is the Boltzmann constant, and $\Delta_0(T)$ is the energy interval between the two components of the KD ground state. Using $\Delta_0 = 36.78 \text{ cm}^{-1} = 4.56 \text{ meV}$, one gets the Sm-Mn exchange interaction $J_6 = 0.27 \text{ meV}$, comparable to $J_6 = 0.7 \text{ meV}$, the expected value of the exchange interaction between $\text{Gd}^{3+} - \text{Mn}^{3+}$ spins in GdMn_2O_5 [21], and an order of magnitude larger than the Dy-Mn interaction in DyMn_2O_5 , $J_6 = 0.06 \text{ meV}$ [20]. Figure 5(b) shows that the normalized $P_s(T)$ has a similar behavior to $\Delta_0(T)$ with respect to their values at 4.5 K. This means that the J_6 Sm-Mn interaction term plays also an important role in the enhancement of P_s in SmMn_2O_5 similar to that recently reported in GdMn_2O_5 [21,23] where the J_6 frustration between the huge and isotropic Gd^{3+} moments and the Mn^{3+} spins is considered responsible for its large extra term in the polarization. We conclude that the microscopic mechanism of the electric polarization in RMn_2O_5 is not only related to $\mathbf{P} \propto \mathbf{C} \mathbf{S}_{\text{Mn}^{3+}} \cdot \mathbf{S}_{\text{Mn}^{4+}}$ exchange striction, as usually claimed, but also depends on an additional $\mathbf{J}_6 \mathbf{S}_{\text{Mn}^{3+}} \cdot \mathbf{S}_{\text{Mn}^{4+}}$ interaction. As in GdMn_2O_5 , we believe that the Sm-Mn symmetric exchange striction is primarily responsible for the large enhancement of the electric polarization in the low ferroelectric phase. The variation of $m_{\text{Sm}}(T)/m_{\text{Sm}}(0)$ is presented in Fig. 5(c). Consistently with what has been reported for some RMn_2O_5 compounds ($R = \text{Ho}, \text{Tb}, \text{Nd}$), where the rare-earth moments are partially ordered well above the presumed $T_N(R)$, here we also find that m_{Sm} is not zero below $T_1 = 34$ K and strongly enhanced below $T_2 \sim 27$ K. Our calculation of $m_{\text{Sm}}(T)/m_{\text{Sm}}(0)$ reproduces perfectly its direct measurement by neutron diffraction below $T_2 \sim 27$ K, using an isotope-enriched ^{154}Sm [22]. This means again that the Sm magnetic order is involved in the magnetic and ferroelectric phases at low temperatures.

The magnetic susceptibility measurements of our samples are presented in Fig. 6(a). Our measurements are in agreement with those reported by Ishii *et al.* [24]. The subtle difference in the scale is probably due to the demagnetization factors. To check whether the phase transitions observed in the magnetic susceptibility measurements are related to the Sm^{3+} ions, we have evaluated the samarium contributions to the magnetic susceptibility $\chi_{\text{Sm}}(T)$ according to the following equation:

$$\chi_{\text{Sm}}^c(T) = N_A \frac{m_{\text{Sm}}^c(0)^2}{k_B T} \frac{1}{\cosh^2[\Delta_0(T)/2k_B T]}, \quad (3)$$

where k_B is the Boltzmann constant and N_A is the Avogadro number. $m_{\text{Sm}}^c(0)$ is the c component of the samarium mag-

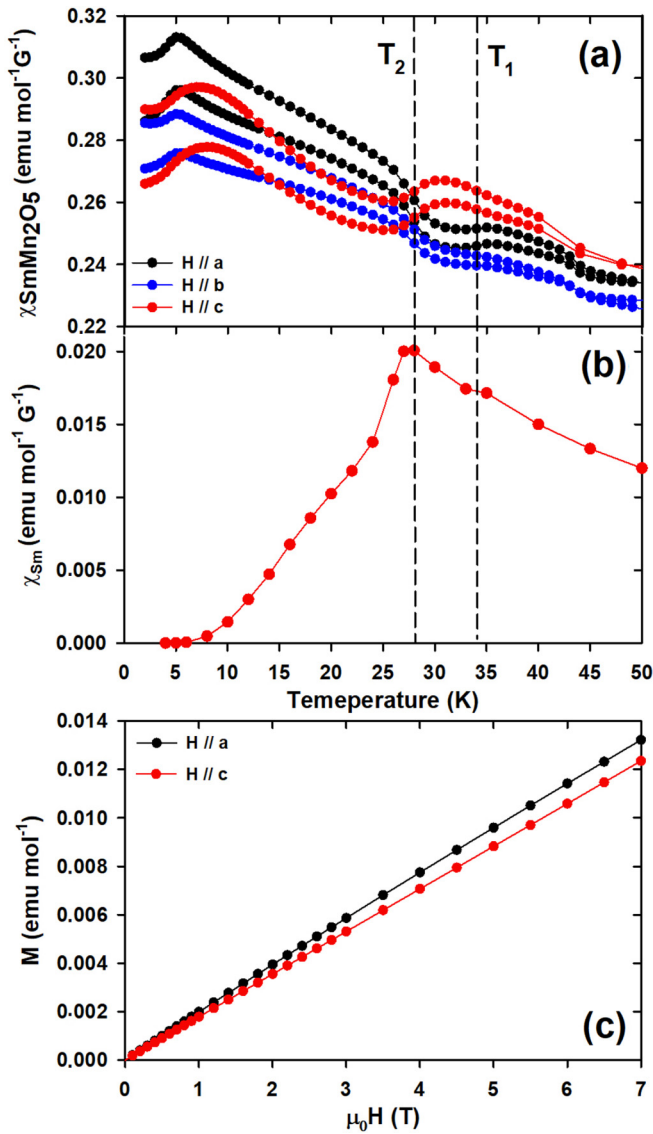


FIG. 6. (a) Magnetic susceptibility of SmMn_2O_5 along the a , b , and c directions. (b) Samarium contribution to the magnetic susceptibility of SmMn_2O_5 calculated according to Eq. (3). (c) Isothermal magnetization curves of SmMn_2O_5 at 2 K for H parallel to a - and c axes.

netic moments. Here, it is considered equal to $0.4 \mu_B$ [22]. The resulting curve is shown in Fig. 6(b) and compared with the $\chi(T)$ (SmMn_2O_5) magnetic susceptibility measurements. The obtained data reveal clearly the antiferromagnetic order of Sm^{3+} magnetic moments below T_2 (weak value of $\chi_{\text{Sm}}(T)$ at 4.5 K: $10^{-6} \text{ emu mol}^{-1} \text{ G}^{-1}$). This result allows us to understand that the subtle slope down of magnetic susceptibility, only observed along the c axis at T_2 , is due to the antiferromagnetic order of Sm^{3+} spins. These observations confirm also that the Sm magnetic moments are aligned along the c axis below T_2 which is consistent with previous findings [22,24]. Isothermal magnetization curves of SmMn_2O_5 at 2 K for H parallel to a - and c axes, presented in Fig. 6(c), exhibit no particular magnetic anisotropy between the two directions.

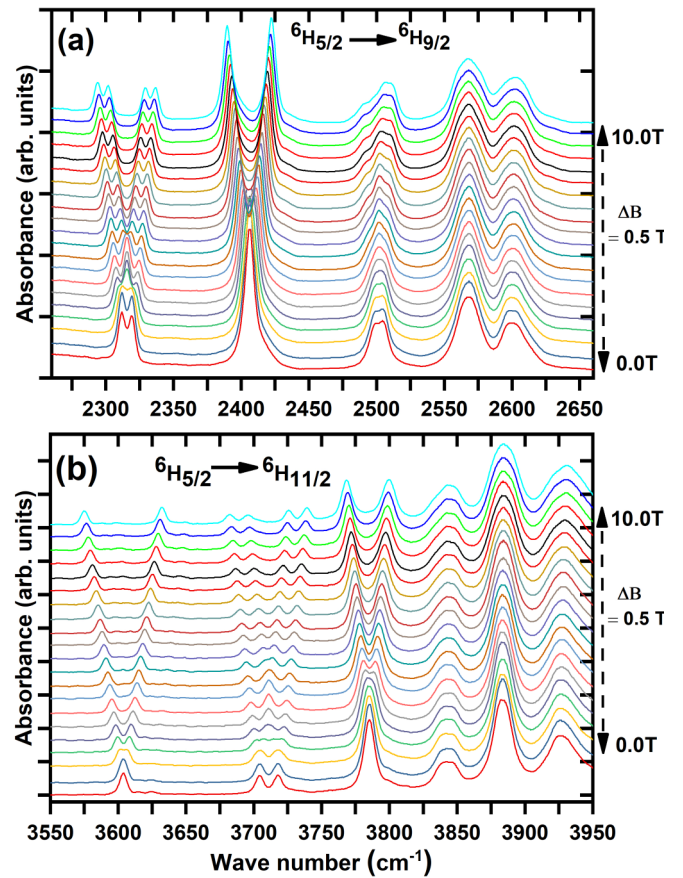


FIG. 7. Magnetic-field dependence of the $\text{Sm}^{3+} \ ^6H_{5/2} \rightarrow \ ^6H_{9/2}$ and $\ ^6H_{5/2} \rightarrow \ ^6H_{11/2}$ CF transitions in SmMn_2O_5 at 4.2 K.

Figure 7 shows the magnetic-field dependence of the $\text{Sm}^{3+} \ ^6H_{5/2} \rightarrow \ ^6H_{9/2}$ and $\ ^6H_{5/2} \rightarrow \ ^6H_{11/2}$ CF transitions in SmMn_2O_5 at 4.2 K. (Additional absorbance maps of $\text{Sm}^{3+} \ ^6H_{5/2} \rightarrow \ ^6H_{11/2}$ CF transitions as a function of magnetic field are presented in Fig. S2(b) reported in the Supplemental Material [35]). Other KD splittings due to the Zeeman effect are detected. At 4.2 K, the high-energy Kramers-doublets component of the ground state is very weakly populated and does not contribute to the CF excitations. Hence the detected splittings are directly due to the KD excited multiplets. Unexpectedly, additional symmetric Zeeman components with the same intensity are clearly observed for some Zeeman CF excitation pairs: (2312 cm^{-1} , 2319 cm^{-1}), (3705 cm^{-1} , 3718 cm^{-1}), (4965 cm^{-1} , 4975 cm^{-1}), (5070 cm^{-1} , 5075 cm^{-1}). For example, the Zeeman components at 2312 and 2319 cm^{-1} split, in their turn, into two other symmetric bands above 1 T. The observation of more than one set of CF excitations under magnetic field is indicative of twinning in the sample generating doublet features. This twinning seems to be symmetric and periodically arranged since they induce symmetric features. Recently, Catalan *et al.* [39] have found that homogeneous gradient stress distribution in PbTiO_3 thin films, induced by the lattice mismatch when the substrate is relaxed through the formation of nanoscale domains (twins), generates a horizontal flexoelectricity that forces the spontaneous polarization to rotate away from the normal. Here, we presume that an

applied magnetic field induces ferroelectric twin domains that could modulate the electric polarization in SmMn_2O_5 . Since there is no information in the literature about the dependence of the electric polarization as a function of magnetic field, further investigation is required to support such scenario.

IV. CONCLUSION

In this paper, we have mainly reported the CF study of Sm^{3+} ion $4f^5$ electron excited states in SmMn_2O_5 . Interestingly, we have found that the ground-state Kramers doublet is resolved into two bands below $T_C = 34$ K. This splitting $\Delta_0(T)$ is strongly enhanced below 27 K, in the low ferroelectric phase. Within the mean-field framework, we have found that $J_6 S_{\text{Mn}^{3+}} \cdot S_{\text{Mn}^{4+}}$ interaction, $J_6 = 0.27$ meV, is involved in the enhancement of Ps of SmMn_2O_5 below 27 K. Using $\Delta_0(T)$, we have also calculated the samarium magnetic moment $m_{\text{Sm}}(T)$ that reproduces well its direct measurement by neutron diffraction using an isotope-enriched ^{154}Sm . The samarium contribution to the magnetic susceptibility is also obtained and compared to the $\chi^c(T)$ (SmMn_2O_5). The

obtained results reveal the antiferromagnetic alignment of the Sm ions moment along the c axis in the low ferroelectric phase. Analyzing all these experimental results, we conclude that the Sm-Mn symmetric exchange striction plays an important role in the large enhancement of the electric polarization in the low ferroelectric phase. The evolution of the Sm^{3+} CF excitations under applied magnetic field is also studied. Interestingly, we have found more than one set of CF excitations, with equivalent intensities. This observation is explained by magnetic-field-induced twinning in the sample that could impact the electric polarization of SmMn_2O_5 .

ACKNOWLEDGMENTS

We acknowledge the technical support of M. Castonguay, S. Pelletier, J. Rousseau, and B. Rivard. S.M., S.J., M.B., and P.F. acknowledge the support from the National Science and Engineering Research Council of Canada, the Fonds de Recherche du Quebec - Nature et Technologies (FRQNT), and Canada Foundation for Innovation. This research was undertaken thanks in part to funding from the Canada First Research Excellence Fund (CFREF).

-
- [1] D. Khomskii, *Physics* **2**, 20 (2009).
- [2] T. Kimura, T. Goto, H. Shintani, K. Ishizaka, T. Arima, and Y. Tokura, *Nature (London)* **426**, 55 (2003).
- [3] N. Hur, S. Park, P. Sharma, J. Ahn, S. Guha, and S.-W. Cheong, *Nature (London)* **429**, 392 (2004).
- [4] S.-W. Cheong and M. Mostovoy, *Nature (London)* **6**, 13 (2007).
- [5] M. Bibes and A. Barthelemy, *Nat. Mater.* **7**, 425 (2008).
- [6] J. A. Mundy, C. M. Brooks, M. E. Holtz, J. A. Moyer, H. Das, A. F. Rébola, J. T. Heron, J. D. Clarkson, S. M. Disseler, Z. Liu, A. Farhan, R. Held, R. Hovden, E. Padgett, Q. Mao, H. Paik, R. Misra, L. F. Kourkoutis, E. Arenholz, A. Scholl, J. A. Borchers, W. D. Ratcliff, R. Ramesh, C. J. Fennie, P. Schiffer, D. A. Muller, and D. G. Schlom, *Nature (London)* **537**, 523 (2016).
- [7] M. J. Pitcher *et al.*, *Science* **347**, 420 (2015).
- [8] I. A. Sergienko and E. Dagotto, *Phys. Rev. B* **73**, 094434 (2006).
- [9] H. Katsura, N. Nagaosa, and A. V. Balatsky, *Phys. Rev. Lett.* **95**, 057205 (2005).
- [10] L. C. Chapon, P. G. Radaelli, G. R. Blake, S. Park, and S.-W. Cheong, *Phys. Rev. Lett.* **96**, 097601 (2006).
- [11] Y. S. Oh, B.-G. Jeon, S. Y. Haam, S. Park, V. F. Correa, A. H. Lacerda, S.-W. Cheong, G. S. Jeon, and K. H. Kim, *Phys. Rev. B* **83**, 060405(R) (2011).
- [12] A. S. Moskvina and R. V. Pisarev, *Phys. Rev. B* **77**, 060102(R) (2008).
- [13] A. S. Moskvina and S.-L. Drechsler, *Phys. Rev. B* **78**, 024102 (2008).
- [14] A. A. Sirenko, S. M. O'Malley, K. H. Ahn, S. Park, G. L. Carr, and S.-W. Cheong, *Phys. Rev. B* **78**, 174405 (2008).
- [15] L. Chaix *et al.*, *Phys. Rev. Lett.* **112**, 137201 (2014).
- [16] O. Prokhnenko, R. Feyerherm, M. Mostovoy, N. Aliouane, E. Dudzik, A. U. B. Wolter, A. Maljuk, and D. N. Argyriou, *Phys. Rev. Lett.* **99**, 177206 (2007).
- [17] O. Prokhnenko, R. Feyerherm, E. Dudzik, S. Landsgesell, N. Aliouane, L. C. Chapon, and D. N. Argyriou, *Phys. Rev. Lett.* **98**, 057206 (2007).
- [18] L. C. Chapon, G. R. Blake, M. J. Gutmann, S. Park, N. Hur, P. G. Radaelli, and S.-W. Cheong, *Phys. Rev. Lett.* **93**, 177402 (2004).
- [19] Z. Y. Zhao, M. F. Liu, X. Li, L. Lin, Z. B. Yan, S. Dong, and J. M. Liu, *Sci. Rep.* **4**, 3984 (2014).
- [20] S. Chattopadhyay, S. Petit, E. Ressouche, S. Raymond, V. Balédent, G. Yahia, W. Peng, J. Robert, M.-B. Lepetit, M. Greenblatt, and P. Foury-Leylekian, *Sci. Rep.* **7**, 14506 (2017).
- [21] G. Yahia, F. Damay, S. Chattopadhyay, V. Balédent, W. Peng, S. W. Kim, M. Greenblatt, M.-B. Lepetit, and P. Foury-Leylekian, *Phys. Rev. B* **97**, 085128 (2018).
- [22] G. Yahia, F. Damay, S. Chattopadhyay, V. Balédent, W. Peng, E. Elkaim, M. Whitaker, M. Greenblatt, M.-B. Lepetit, and P. Foury-Leylekian, *Phys. Rev. B* **95**, 184112 (2017).
- [23] N. Lee, C. Vecchini, Y. J. Choi, L. C. Chapon, A. Bombardi, P. G. Radaelli, and S.-W. Cheong, *Phys. Rev. Lett.* **110**, 137203 (2013).
- [24] Y. Ishii, S. Horio, M. Mitarashi, T. Sakakura, M. Fukunaga, Y. Noda, T. Honda, H. Nakao, Y. Murakami, and H. Kimura, *Phys. Rev. B* **93**, 064415 (2016).
- [25] M. Tachibana, K. Akiyama, H. Kawaji, and T. Atake, *Phys. Rev. B* **72**, 224425 (2005).
- [26] D. Barba, S. Jandl, V. Nekvasil, M. Maryško, K. Jurek, M. Diviš, and Th. Wolf, *Phys. Rev. B* **69**, 024528 (2004).
- [27] S. Mansouri, S. Jandl, B. Roberge, M. Balli, D. Z. Dimitrov, M. Orlita, and C. Faugeras, *J. Phys.: Condens. Matter* **28**, 055901 (2016).
- [28] S. Mansouri, S. Jandl, A. Mukhin, V. Y. Ivanov, and A. Balbashov, *Sci. Rep.* **7**, 13796 (2017).
- [29] S. Jandl, S. Mansouri, J. Vermette, A. A. Mukhin, V. Yu Ivanov, A. Balbashov, and M. Orlita, *J. Phys.: Condens. Matter* **25**, 475403 (2013).
- [30] S. Mansouri, S. Jandl, M. Balli, P. Fournier, A. A. Mukhin, V. Yu Ivanov, A. Balbashov, and M. Orlita, *J. Phys.: Condens. Matter* **30**, 175602 (2018).

- [31] S. Mansouri, S. Jandl, M. Balli, J. Laverdiere, P. Fournier, and D. Z. Dimitrov, *Phys. Rev. B* **94**, 115109 (2016).
- [32] B. M. Wanklyn, *J. Mater. Sci.* **7**, 813 (1972).
- [33] H. Kimura, S. Kobayashi, Y. Fukuda, T. Osawa, Y. Kamada, Y. Noda, I. Kagomiya, and K. Kohn, *J. Phys. Soc. Jpn.* **76**, 074706 (2007).
- [34] S. Mansouri, S. Jandl, M. Balli, P. Fournier, B. Roberge, M. Orlita, I. A. Zobkalo, S. N. Barilo, and S. V. Shiryaev, *Phys. Rev. B* **98**, 205119 (2018).
- [35] See Supplemental Material at <http://link.aps.org/supplemental/10.1103/PhysRevB.100.085147> for the variation of the Sm^{3+} ${}^6H_{5/2} \rightarrow {}^6H_{9/2}$ CF transitions as a function of temperature and magnetic field.
- [36] V. Baledent, S. Chattopadhyay, P. Fertey, M. B. Lepetit, M. Greenblatt, B. Wanklyn, F. O. Saouma, J. I. Jang, and P. Foury-Leylekian, *Phys. Rev. Lett.* **114**, 117601 (2015).
- [37] T. A. Tyson, M. Deleon, S. Yoong, and S.-W. Cheong, *Phys. Rev. B* **75**, 174413 (2007).
- [38] T. C. Han, J. G. Lin, K. M. Kuo, and G. Chern, *J. Appl. Phys.* **103**, 084106 (2008).
- [39] G. Catalan, A. Lubk, A. H. G. Vlooswijk, E. Snoeck, C. Magen, A. Janssens *et al.*, *Nat. Mater.* **10**, 963 (2011).